


Kinetics, isotherm, and thermodynamic studies of methylene blue adsorption from water by *Mytella falcata* waste

Társila S. Silva¹ · Lucas Meili¹  · Sandra Helena V. Carvalho¹ · João Inácio Soletti¹ · Guilherme Luiz Dotto² · Eduardo Jorge S. Fonseca³

Received: 23 January 2017 / Accepted: 26 June 2017 / Published online: 8 July 2017
© Springer-Verlag GmbH Germany 2017

Abstract This work evaluates the application of *Mytella falcata* shells, discarded in large quantities in the state of Alagoas, Brazil, as adsorbent for methylene blue dye (MB). It was investigated how the amount of adsorbent (M), the average particle diameter (G), and the agitation speed (A) affected the adsorption. Kinetic and equilibrium studies were conducted, and the pseudo-second-order equation adequately represented the kinetic data and isotherms following Liu's model ($q_{\max} = 8.81 \text{ mg g}^{-1}$ at 60 °C). The adsorption was spontaneous, favorable, and endothermic. *Mytella falcata* shell is a suitable adsorbent for MB and could potentially contribute to its removal from the environment.

Keywords Clamshell · Waste · Dyes · Removal · Alternative adsorbents

Introduction

The wastewater from textile industries contains considerable amounts of dyes that are not easily biodegradable in natural

environments. The direct discharge of colored effluents containing toxic components is hazardous to the environment: they diminish sunlight penetration into water bodies, which harms the photosynthesis activity of plants and the growth of biota (Gad and El-Sayed 2009). Furthermore, synthetic dyes display toxic, mutagenic, and carcinogenic effects, which can affect the human life negatively (Carneiro et al. 2010). Several techniques such as coagulation, oxidation, biodegradation, photolysis, filtration, and adsorption can remove dyes from wastewater (Fernandez et al. 2010). In particular, adsorption is a simple process that relies on the availability of a wide range of adsorbents, which make this process an effective method to reduce the concentration of dissolved dyes in industrial effluents. Adsorption transfers the dyes present in an aqueous effluent to a solid phase, significantly decreasing the bioavailability of the dyes to living organisms (Treviño-Cordero et al. 2013; Wang and Li 2013; Zhang et al. 2013). Subsequently, the adsorbent can be regenerated or stored in a dry place without direct contact with the environment, and the decontaminated effluent can be released into the environment (Machado et al. 2011).

In this context, interest in alternative effective and inexpensive adsorbents for dye removal has increased. Babaçu coconut (Vieira et al. 2009), cupuaçu shell (Cardoso et al. 2011), sugarcane bagasse (Zhang et al. 2013), rice bran (Suzuki et al. 2007), papaya seeds (Paz et al. 2013; Weber et al. 2013), bottle gourd (Foletto et al. 2012), oyster shell (Asaoka et al. 2009), moringa aptera Gaertn (Matouq et al. 2015), Persian olive (Rahimdokht et al. 2016), *Cyclosorus interruptus* (Zhou et al. 2015), castor bean presscake (Magriotis et al. 2014), raw peach shell (Markovic et al. 2015), neem (*Azadirachta indica*) leaf powder (Bharali and Bhattacharyya 2015), shell dust of the snail *Physa acuta* (Hossain and Aditya 2013), untreated and mussel shell-treated granitic material (Otero et al. 2015), waste shell dust of fresh water mussel

Responsible editor: Philippe Garrigues

✉ Lucas Meili
lucas.meili@ctec.ufal.br

¹ Separation Systems and Process Optimization Laboratory, Center of Technology, Federal University of Alagoas, Maceió, AL 57072-970, Brazil

² Environmental Processes Laboratory (LAPAM), Chemical Engineering Department, Federal University of Santa Maria, Santa Maria, RS 97105-900, Brazil

³ Quantic and Non Linear Optic Laboratory, Department of Physics, Center of Exact and Natural Sciences, Federal University of Alagoas, Maceió, AL 57072-970, Brazil

Lamellidens marginalis (Hossain et al. 2015), bivalve mollusk shell (Yousefi et al. 2015), biochar from biofuel residue (Yao et al. 2015), hickory and peanut hull hydrochars (Fang et al. 2016), un-amended and amended mussel shell (Garrido-Rodriguez et al. 2014), and calcined mussel shell (El Haddad et al. 2014) are examples of alternative adsorbents.

“Sururu” (*Mytella falcata*) is well known in the state of Alagoas (Brazil) and is even considered a symbol of the region. According to the Federation of Fishermen of Alagoas, 10,000 people survive on the collection of mussels, both for subsistence and for sale (OPAS 2015). Sururu collection is an activity that generates large amounts of waste. Irregular exploitation of mussels and incorrect waste disposal have caused several environmental problems. According to the Ministry of Fisheries and Aquaculture (Brazil) (MPA 2015), in 2011 mussels were the most captured species (3772.5 t) among clams, followed by sururu (2133.3 t) and octopus (2089.6 t). In the Alagoas area, “maçunim” (another mollusk species) was the most captured species (317.4 t), followed by sururu (217.9 t) and oyster (95.8 t).

This work aimed to evaluate the adsorptive capacity of *M. falcata* shells, a solid waste, widely generated that causes several environmental problems due to its inadequate management, for removal of methylene blue dye. Specific surface area (BET) measurements, scanning electron microscopy (SEM), infrared spectroscopy (FT-IR), X-ray diffraction (XRD), thermogravimetric analysis (TGA), and X-ray-dispersive energy spectroscopy (EDS) aided characterization of the material. To determine the applicability of the adsorbent, a 2³ full experimental design was performed to investigate how the amount of adsorbent (M), the average particle diameter of the adsorbent (G), and the agitation speed affected the adsorption process. The pseudo-first-order and pseudo-second-order models were used to fit the kinetic data. The Langmuir, Freundlich, Liu, and Redlich-Peterson models were employed to fit the adsorption equilibrium data. Thermodynamic parameters like activation energy, standard enthalpy change, standard Gibbs energy change, and standard entropy change were determined.

Materials and methods

Chemicals

Methylene blue dye (MB) (Sigma-Aldrich, molecular formula = C₁₆H₁₈N₃SCl, purity = 99%, molecular weight = 319.86, C. I. = 52,015) was used in this work (Ezzeddine et al. 2016; Samal et al. 2017). This cationic dye is common in paint and textile effluents. For the adsorption assays, all the solutions were prepared with distilled water, and all the reagents were of analytical grade. MB was quantified by a UV-visible spectrophotometer (Shimadzu, UVmini-1240, Japan) at 665 nm (Paz et al. 2013).

Adsorbent

The *M. falcata* (mussels) shell was used as adsorbent. The raw material was collected in “Sururu de Capote” community (Maceió/Alagoas/Brazil). Figure 1 shows the discarded *M. falcata* shells. The shells were washed to remove the mud, and the material was placed in an oven at 60 °C for 8 h, to reduce the moisture content. The shells were then crushed in an industrial blender and classified by a Tyler series sieves. Figure 2a illustrates the shells without crushing. Figure 2b, c shows the shells with average particle sizes of 0.443 mm and smaller than 0.149 mm, respectively.

Adsorbent characterization

Specific surface area (BET) measurements, scanning electron microscopy (SEM), infrared spectroscopy (FT-IR), X-ray diffraction (XRD), thermogravimetric analysis (TGA), and X-ray-dispersive energy spectroscopy (EDS) were used to characterize the material with the smallest particle size (<0.149 mm). The functional groups of the shells were identified by FT-IR (Varian 660 IR). The thermal profile was obtained by TGA (Shimadzu/TGA 50 coupled to a thermal analyzer TA60WS). The crystal structure was determined by XRD (Shimadzu/XRD-6000). The surface morphology was analyzed by SEM (Shimadzu/SSX-550). The adsorbent was characterized by N₂ adsorption-desorption isotherms at 77 K on Micromeritics ASAP 2020 equipment operating at relative pressure (P/P₀) ranging from 0.01 to 0.99. Elements present in the material were qualitatively and quantitatively determined by EDS (Shimadzu/EDS 800HS) (Viriya-empikul et al. 2010).

Experimental design for batch experiments

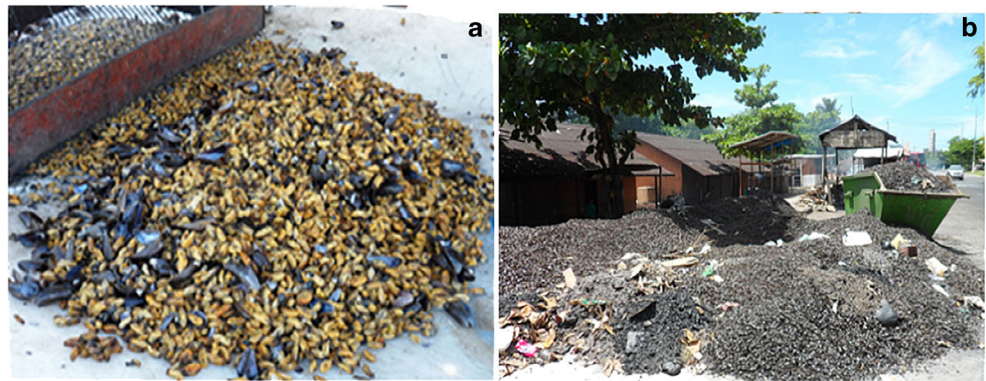
A 2³ experimental design was used to perform the batch experiments. To this end, 25 mL of MB dye solution at an initial concentration of 100 mg L⁻¹ and the adsorbent were placed in flasks. The mixture (dye solution + adsorbent) was stirred in a shaker incubator at an average temperature of 25 °C and residence time of 60 min. After adsorption, an aliquot of the solution was withdrawn, and the final MB concentration in solution was determined by spectrophotometry.

The input variables were the amount of adsorbent (M), the average particle diameter of the adsorbent (G), and agitation speed (A). Table 2 presents the levels. The experiments were performed in duplicate, in random order. The adsorption capacity (*q*) was the considered response, given by Eq. 1:

$$q = \frac{C_0 - C_f}{M} V \quad (1)$$

where *C*₀ is the initial MB concentration (mg L⁻¹), *C*_f is the final MB concentration (mg L⁻¹) at 60 min, *V* is the volume of the solution (L), and *M* is the amount of adsorbent (g).

Fig. 1 **a** *Mytella falcata*. **b** The disposal of shells in Maceió/AL/ Brazil



Kinetic and equilibrium experiments

The kinetic curves were constructed in batch systems at 25 °C and 200 rpm in a shaker incubator. Briefly, 25 mL of MB solutions of different initial MB concentrations (25, 100, and 200 mg L⁻¹) was added to the flasks containing 0.5 g of adsorbent with particle size <0.149 mm. After the predetermined time, an aliquot (without the presence of the adsorbent) was removed and quantified on a spectrophotometer.

Equilibrium studies were performed in a finite bath system; 0.5 g of adsorbent (particle size <0.149 mm) was employed. The MB solutions (concentrations ranging from 10 to 600 mg L⁻¹) were placed in contact with the adsorbent for 50 min under constant agitation of 200 rpm in a shaker incubator working at different temperatures (25, 40, 50, and 60 °C) (Chowdhury and Saha 2010). After 50 min, aliquots were withdrawn and quantified in a spectrophotometer. All the experiments were performed in duplicate.

Modeling

From the kinetic viewpoint, MB adsorption onto *M. falcata* (mussels) shells was investigated by using the pseudo-first-order (Lagergren 1898) (Eq. 2) and pseudo-second-order (Ho and McKay 1998a, b, 1999) (Eq. 3) models:

$$q_t = q_1(1 - \exp(-k_1t)) \tag{2}$$

$$q_t = \frac{t}{(1/k_2q_2^2) + (t/q_2)} \tag{3}$$

$$q_t = \frac{V(C_0 - C_t)}{m} \tag{4}$$

Fig. 2 *Mytella falcata* shells **a** without milling, **b** 0.443 mm, and **c** <0.149 mm



where k_1 and k_2 are the rate constants of the pseudo-first-order and pseudo-second-order models (in min⁻¹ and g mg⁻¹ min⁻¹, respectively), q_1 and q_2 are the theoretical values for the adsorption capacity (mg g⁻¹), t is the time (min), and q_t is the adsorption capacity determined by Eq. 4, where q_t (mg g⁻¹) is the quantity of adsorbed MB, C_t (mg L⁻¹) is the MB concentration in the liquid phase at any time, C_0 (mg L⁻¹) is the initial dye concentration, V is the volume of the solution (L), and m is the amount of adsorbent (g).

Regarding the equilibrium, Langmuir (1918) (Eq. 5), Freundlich (1906) (Eq. 6), Liu et al. (2003) (Eq. 7), and Redlich-Peterson (Redlich and Peterson 1959) (Eq. 8) models were used:

$$q_e = \frac{q_m K_L C_e}{1 + (K_L C_e)} \tag{5}$$

$$q_e = K_F C_e^{1/n_F} \tag{6}$$

$$q_e = \frac{q_S (K_S C_e)^{m_S}}{1 + (K_S C_e)^{m_S}} \tag{7}$$

$$q_e = \frac{K_{RP} C_e}{1 + (a_{RP} C_e)^\beta} \tag{8}$$

where q_e is the adsorption capacity in the equilibrium, calculated by Eq. 1, q_m is the maximum adsorption capacity (mg g⁻¹), K_L is the Langmuir constant (L mg⁻¹), K_F is the Freundlich constant (mg g⁻¹)(mg L⁻¹)^{-1/n_F}, $1/n_F$ is the heterogeneity factor, q_S is the maximum adsorption capacity from the Liu model (mg g⁻¹), K_S is the Liu constant (L mg⁻¹), m_S is the exponent of the Liu model, and K_{RP} (L mg⁻¹) and a_{RP} (L mg⁻¹)^β and β are the Redlich-Peterson constants.

Results

Adsorbent characterization

Figure 3 presents the FT-IR vibrational spectrum of the *M. falcata* shell. The main intense bands emerged at 3360, 2925, 2850, 2520, 1784, 1466, 1078, 854, and 705 cm^{-1} . The FT-IR spectrum contained the characteristic bands of crystalline aragonite (CaCO_3), which is typical of mollusk shells. The vibration modes at 705, 854, 1078, and 1466 cm^{-1} attested that the carbonate group was present in the shell. The band at 705 cm^{-1} corresponded to angular deformations in the OCO connection plane. The band at 854 cm^{-1} referred to angular deformations outside the connection plane of CO_3 . The band at 1078 cm^{-1} was attributed to symmetric stretching of the CO bond. The band at 1466 cm^{-1} was due to asymmetric stretching of the CO bond. The band at 2520 cm^{-1} indicated that resident radical HCO_3^- existed in the material. The bands at 2850 and 2925 cm^{-1} were associated with the CH vibrational modes of various organic matter species present in the sample. The band near 3400 cm^{-1} corresponded to water OH stretching originating from moisture in the sample. The spectral data resembled the results reported by Li et al. (2012) and Silva et al. (2010).

Figure 4 depicts the X-ray diffractogram of the shell and confirmed its carbonaceous nature. The shell displayed high calcium concentration and contained carbon and oxygen. The XRD patterns revealed that the shell comprised the crystalline forms of calcium carbonate (CaCO_3), aragonite, and calcite, which are the main constituents of shellfish shells. The percentage of aragonite and calcite phases may vary depending on the mollusk and the region where the species developed. According to Silva et al. (2010), crystallographic characterization of mollusk shells cannot always determine the proportions of the different calcium carbonate crystalline phases in shells because textures are different and the material may contain mixtures of other organic and amorphous impurities. The XRD results corroborated with the infrared data recorded for the *M. falcata* shell in Fig. 3.

Figure 5 shows the curve of the weight loss versus temperature (A) and the differential thermal analysis curve as a function of temperature (B). Based on curve (A), significant weight loss occurred between 650 and 800 $^\circ\text{C}$ due to calcium carbonate (CaCO_3) decarbonation, and calcium oxide (CaO) formation. Differential thermal analysis (DrTGA) (B) evidenced a peak at approximately 785 $^\circ\text{C}$, which indicated CaO formation (Silva et al. 2010). Figure 5, curve (A), illustrates how weight loss evolved from 30 to 900 $^\circ\text{C}$. Organic content degradation

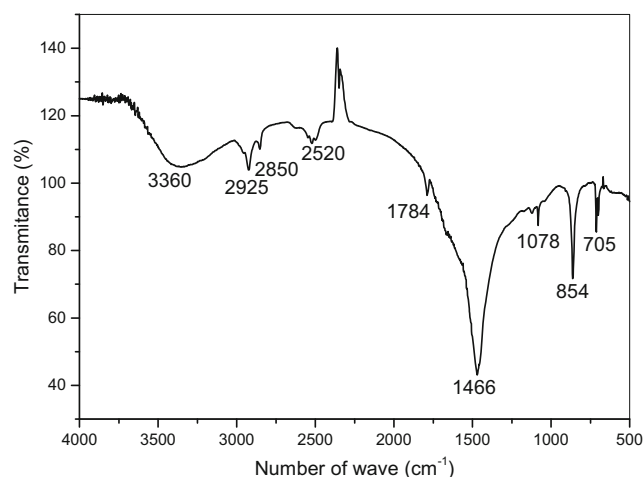


Fig. 3 FT-IR vibrational spectrum

took place around 200 $^\circ\text{C}$, and the percentage of weight loss was about 9%. Total weight loss was approximately 43% around 650 $^\circ\text{C}$. According to Mohamed et al. (2012), the results agreed with the theoretical decomposition of calcium carbonate, $\text{CaCO}_3 \rightarrow \text{CaO} + \text{CO}_2$. Assuming that there were no impurities, CaCO_3 degradation produced approximately 40 and 60%, by weight, of CaO and CO_2 , respectively.

Figure 6 brings the micrographs of the shells in different forms, cross section, and powder, obtained by SEM. Figure 6a, b shows the details of the cross section, revealing the overlapping lamellae that form the body of the *M. falcata* shell. Figure 6c, d displays the inner surface, where particle size distribution is more heterogeneous, and Fig. 6e, f shows the structure of the powder exhibiting smaller particles. Li et al. (2012) and Dauphin et al. (2013) also observed this morphological characteristic—lamellar structures—for bivalve mollusks.

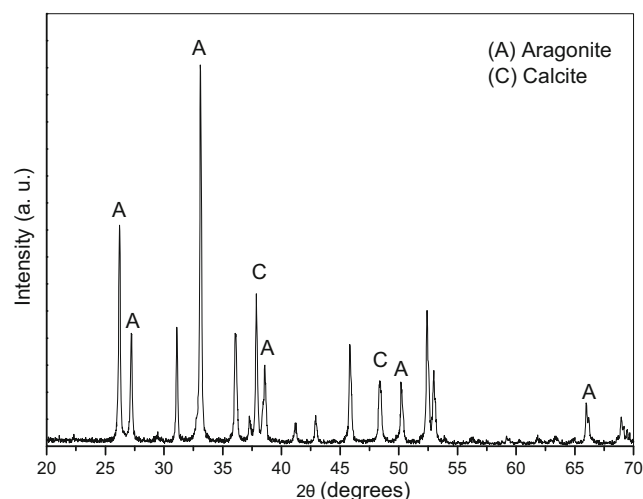
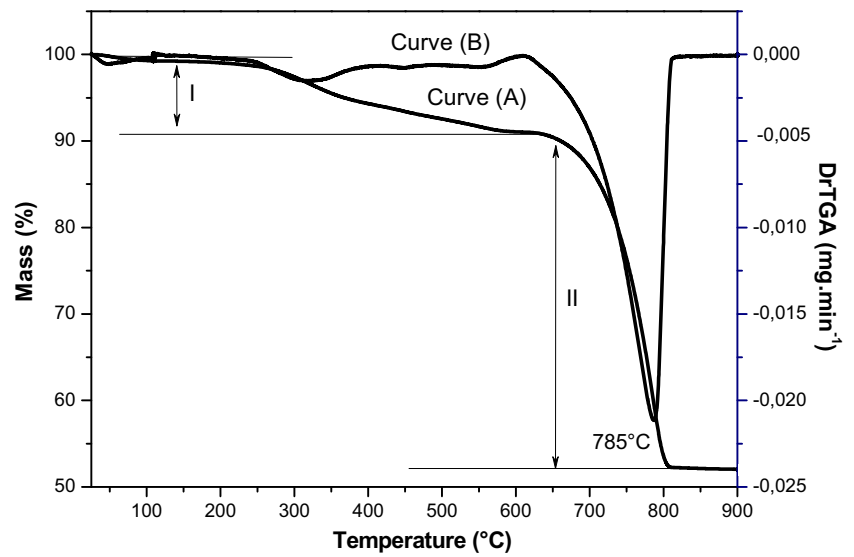


Fig. 4 XRD pattern. A Aragonite and C calcite

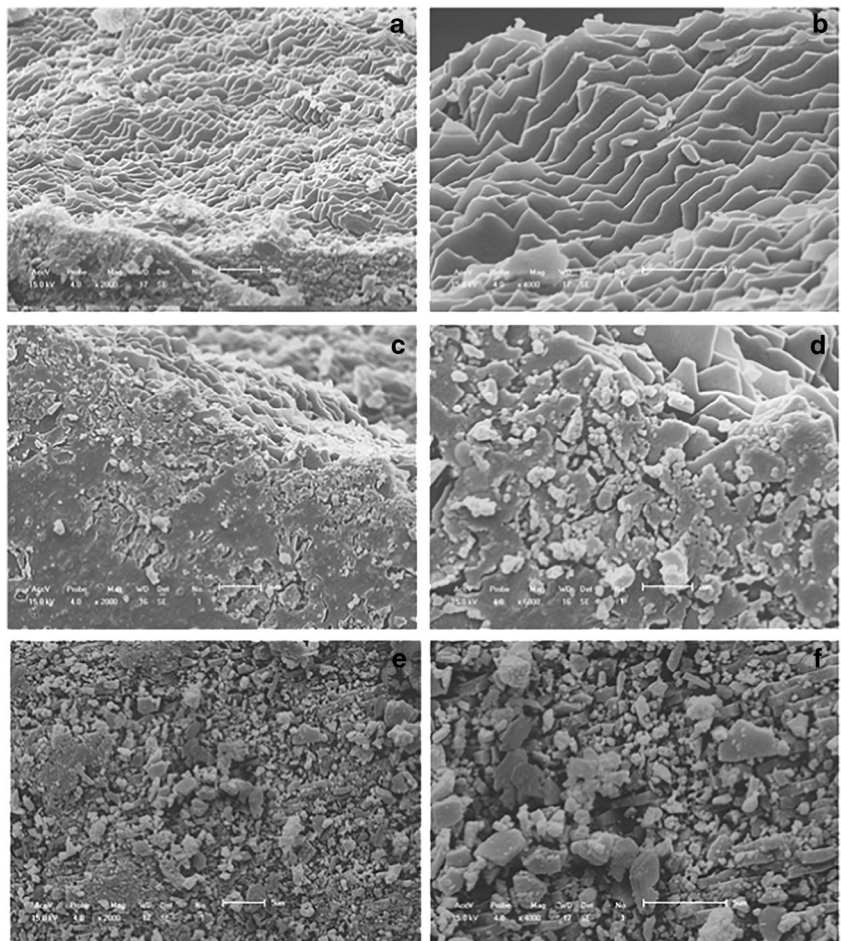
Fig. 5 A TGA and B DrTG curves



The specific surface area, the total pore volume, and the average diameter of the pores were 65 m²/g, 0.0676 cm³/g, and 41 Å, respectively, as determined by N₂ adsorption/

desorption (BET). The specific surface area was high as compared to other mollusks reported in the literature, such as the bivalve mollusk shell from beaches in India (3.6 m²/g)

Fig. 6 SEM images. **a, b** Shell surface. **c, d** Lamellae. **e, f** Internal surface



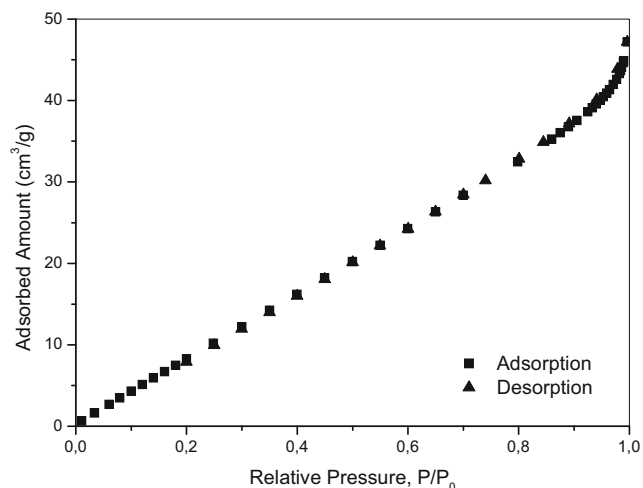


Fig. 7 N₂ adsorption/desorption isotherm at 77 K

(Chowdhury and Saha 2010). Figure 7 corresponds to the N₂ adsorption/desorption isotherm at 77 K and shows that the isotherm profile was type II, without hysteresis. According to the IUPAC classification, this profile is typical of non-porous solid. However, the absence of hysteresis does not mean porosity is absent because some kinds of pores may lead to adsorption and desorption (Webb and Orr 1997). The surface area analysis results confirmed the morphology viewed by the SEM technique (Fig. 6) and attested that the *M. falcata* shell was not porous, but lamellar.

EDS analyses afforded the elemental composition of the *M. falcata* shell as shown in Table 1. The material contained high concentration of calcium (Ca) and much smaller proportions of sodium (Na), phosphorus (P), sulfur (S), strontium (Sr), iron (Fe), silicon (Si), and chromium (Cr), corroborating the previous results.

Experimental design

Table 2 depicts the 2³ experimental design matrix with the average values of *q_e* in each combination of levels for the

Table 1 *Mytella falcata* shell composition by EDS

Composition	Percentage
Ca	91.8
Na	3.2
P	1.6
S	1.4
Sr	1.1
Fe	0.5
Si	0.3
Cr	0.1

Table 2 Experimental design matrix

Run	Mass (g)	Average diameter (mm)	Agitation (rpm)	<i>q_e</i> (mg g ⁻¹)
1	-1 (0.5)	-1 (<0.149)	-1 (50)	2.8
2	+1 (3.0)	-1 (<0.149)	-1 (50)	0.5
3	-1 (0.5)	+1 (0.443)	-1 (50)	1.2
4	+1 (3.0)	+1 (0.443)	-1 (50)	0.4
5	-1 (0.5)	-1 (<0.149)	+1 (200)	3.1
6	+1 (3.0)	-1 (<0.149)	+1 (200)	0.8
7	-1 (0.5)	+1 (0.443)	+1 (200)	1.1
8	+1 (3.0)	+1 (0.443)	+1 (200)	0.5

input variables. The results were fitted to a linear model, leading to an empirical correlation that described the adsorption capacity. Table 3 summarizes the effects calculated from the input variables on the response variable and provides the standard errors. The variable that influenced the adsorption process the most was the amount of adsorbent (M), followed by the average particle diameter of the adsorbent (G) and the effect of the interaction between the mass of adsorbent (M) and the average particle diameter of the adsorbent (G).

Equation 9 represents the empirical model obtained by linear regression of the experimental data:

$$q_e = 1.29 - 0.75x_M - 0.52x_G + 0.07x_A + 0.40x_Mx_G \tag{9}$$

where *x_M*, *x_G*, and *x_A* are the amount of adsorbent, the average particle diameter of the adsorbent, and the agitation speed, respectively.

The second and the third terms in Eq. 9 influence the amount of adsorbed dye negatively. When the amount of adsorbent and the average particle diameter of the adsorbent increased, the response variable value (*q_e*) decreased. In contrast, according to the fourth term of Eq. 9, the

Table 3 The estimated effects and their standard errors

Variables	Effect	Standard error (±)	<i>p</i>
Average value	1.29	0.03	0.000
1: Mass	-1.50	0.05	0.000
2: Average diameter	-1.03	0.05	0.000
3: Agitation	0.15	0.05	0.015
1*2	0.79	0.05	0.000
1*3	0.04	0.05	0.472
2*3	-0.11	0.05	0.058
1*2*3	0.04	0.05	0.416

Table 4 ANOVA table

Variation source	Sum of squares (SS)	Degrees of freedom	Mean square (MS)
Regression	15.88	4	3.97
Residues	0.09	11	0.01
Lack of adjustment	0.01	3	0.00
Pure error	0.07	8	0.01
Total	16.05	15	–
R^2	0.995	–	–

variable agitation speed affected the response variable positively: increasing agitation increased the amount of adsorbed dye. The maximum amount of adsorbed MB was 3.11 mg g^{-1} under the following conditions: mass of adsorbent (M) = 0.5 g, particle diameter of adsorbent (G) <0.149 mm, and agitation speed (A) = 200 rpm. These optimal values were used in the subsequent tests.

The ANOVA table—analysis of variance—in Table 4 confirmed the adequacy of the empirical model represented by Eq. 9.

Comparison of the F_{tab} (3.36, 95% of confidence) and F_{calc} (39.7) values, with $F_{\text{calc}} > F_{\text{tab}}$, showed that the described model was valid. The coefficient of determination (R^2) was 0.99, close to unit, and the values of the lack of fit and pure error were low, indicating the model was well adjusted to the experimental data.

Kinetic and equilibrium studies

Figure 8 shows that MB adsorption onto the *M. falcata* shell was fast. Equilibrium was reached after 30 min, revealing good efficiency (Ruthven 1984). The time

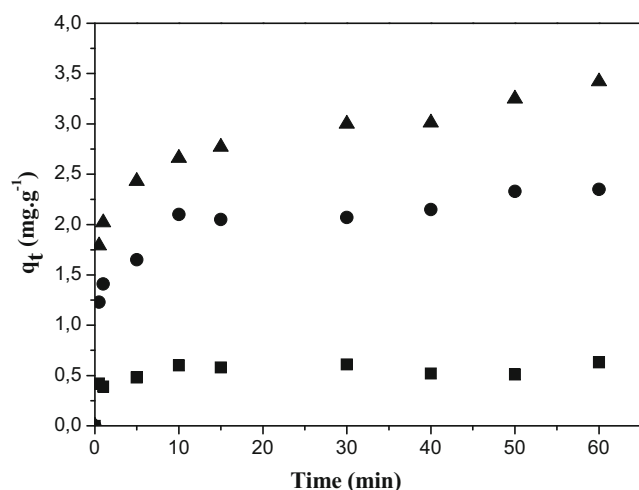


Fig. 8 Kinetic curve for MB adsorption onto *Mytella falcata* shell at 25 °C: filled triangle, 25 ppm; filled circle, 100 ppm; and filled square, 200 ppm

necessary for equilibrium to be reached did not depend on the studied concentrations. The experimental data fitted with non-linear pseudo-first-order and pseudo-second-order models (Russo et al. 2015). Table 5 contains data regarding the kinetic constants and the statistical values. The coefficients of determination were near unit ($R^2 > 0.91$) for the three studied concentrations. Furthermore, the q_{calc} values were close to q_{exp} values, enhancing the applicability of the pseudo-second-order model. El Haddad et al. (2014) and Chowdhury and Saha (2010) obtained similar results.

Figure 9 displays the adsorption isotherms. An increase in temperature favored MB adsorption, demonstrating that the process had endothermic characteristics. The Langmuir, Freundlich, Redlich-Peterson, and Liu isotherm models were evaluated. Table 6 lists the results. The Liu model was the best fit for all the evaluated temperatures, then was the most suitable to describe MB adsorption onto the *M. falcata* shell. The amount of adsorbed dye (q_e) is another parameter that can be used as adjusting evaluator of the models. The q_{max} values obtained by the Liu model (3.01, 6.35, 7.77, and 9.53 mg g^{-1}) were close to the q_{exp} values (3.29, 6.11, 7.28, and 8.81 mg g^{-1}) recorded at temperatures of 25, 40, 50, and 60 °C, respectively.

Thermodynamics

The Arrhenius equation (Eq. 10) afforded the activation energy (E_a)

$$\ln k = \ln A - \frac{E_a}{RT} \tag{10}$$

where k is the constant of velocity, which was 0.866, 0.424, and 0.238 at 25, 40, and 60 °C, respectively; A is the Arrhenius constant, E_a is the activation energy (kJ mol^{-1}), R is the constant of gases ($8.314 \text{ J mol}^{-1} \text{ K}^{-1}$), and T is the temperature (K). The activation energy can be determined from the graph slope of $\ln k$ as a function of $1/T$.

Table 5 Kinetic parameters

C (ppm)	$q_{e \text{ exp}}$ (mg g^{-1})	Pseudo-first-order				Pseudo-second-order			
		$q_{e \text{ calc}}$ (mg g^{-1})	k_1 (min^{-1})	Error	R^2	$q_{e \text{ calc}}$ (mg g^{-1})	k_2 ($\text{g mg}^{-1} \text{min}^{-1}$)	Error	R^2
25	0.5171	0.5562	2.012	0.02410	0.8794	0.5693	6.567	0.02215	0.9146
100	2.147	2.094	1.400	0.08248	0.9073	2.177	0.9191	0.06850	0.9499
200	3.011	2.925	1.502	0.1212	0.8964	3.035	0.7225	0.1042	0.9393

The thermodynamic parameters such as standard Gibbs free energy change (ΔG^0), standard enthalpy change (ΔH^0), and standard entropy change (ΔS^0) were evaluated from the adsorption isotherms. Analysis of the thermodynamic parameters under equilibrium conditions provides significant information about the adsorption process. To obtain the thermodynamic parameters, it is necessary to determine the thermodynamic equilibrium

constant (K_e), represented by Eq. 11, and to calculate the parameters using Eqs. 12 and 13 (Tan et al. 2008).

$$K_e = \rho \cdot k_s \cdot q_s \quad (11)$$

$$\Delta G^0 = -R \cdot T \cdot \ln K_e \quad (12)$$

$$\Delta G^0 = \Delta H^0 - T \cdot \Delta S^0 \quad (13)$$

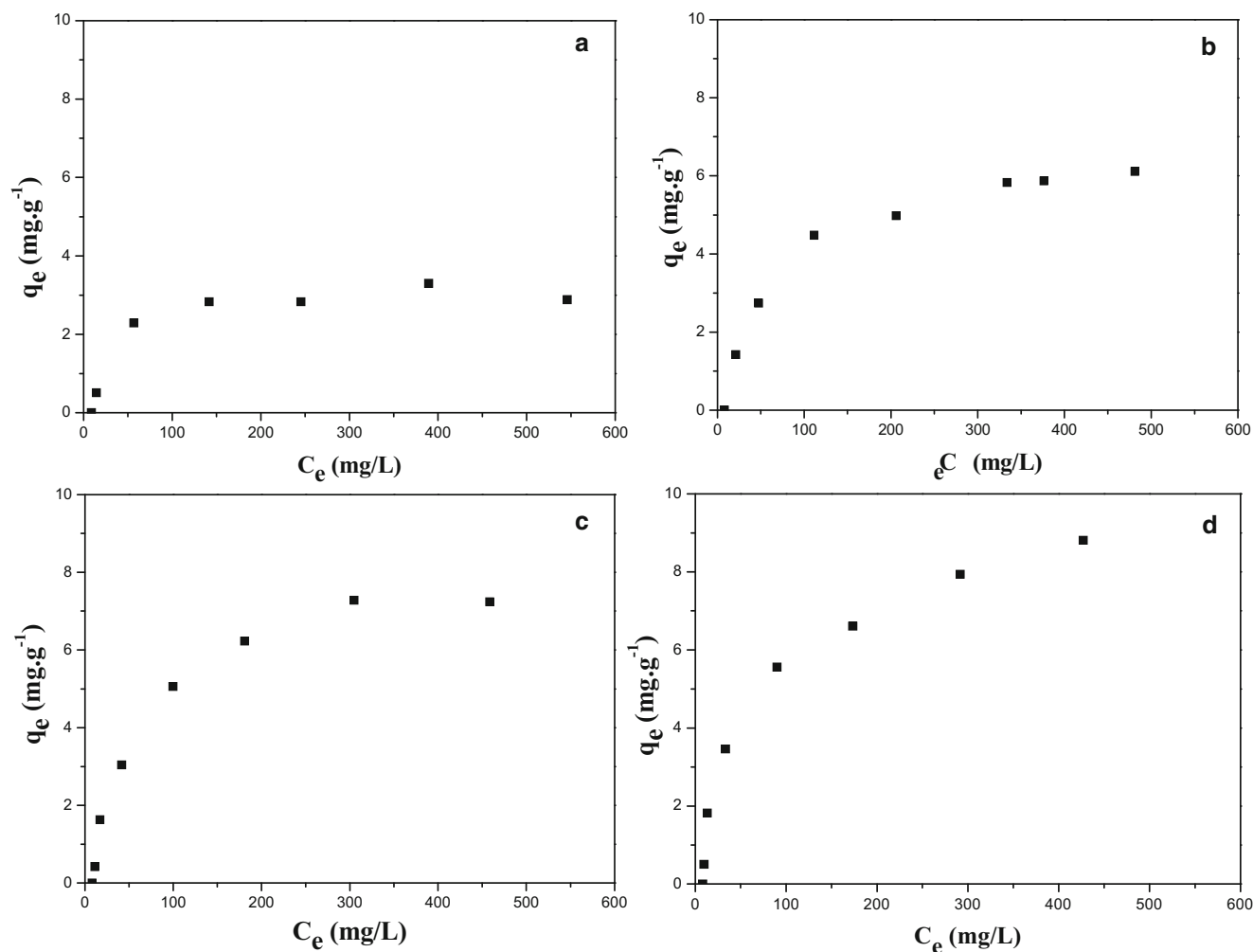


Fig. 9 Equilibrium curves for MB adsorption onto *Mytella falcata* shell: **a** 25 °C, **b** 40 °C, **c** 50 °C, and **d** 60 °C

Table 6 Isotherm parameters

Model	Parameter	25 °C	40 °C	50 °C	60 °C
Langmuir	q_{max} (mg g ⁻¹)	3.514	7.202	9.079	10.29
	K_L (L mg ⁻¹)	0.02030	0.01218	0.01136	0.01209
	Standard error	0.3542	0.3643	0.6496	0.7787
	R^2	0.9109	0.9814	0.9764	0.9738
Freundlich	N	2.913	2.359	2.155	2.108
	K_F [(mg L ⁻¹)(L g ⁻¹) ^{1/n}]	0.4033	0.4843	0.4826	0.5340
	Standard error	0.2682	0.4149	0.4059	0.3337
	R^2	0.7293	0.9098	0.8912	0.9224
Redlich-Peterson	K_R	0.04995	0.07551	0.08025	0.1256
	a_R (L mg ⁻¹) ^β	2.0.10 ⁻³	5.0.10 ⁻³	1.8.10 ⁻³	0.01274
	β	1.292	1.119	1.259	0.9929
	Standard error	0.4574	0.2036	0.2023	0.2444
	R^2	0.9326	0.9805	0.9811	0.9685
Sips	q_s (mg g ⁻¹)	3.011	6.355	7.771	9.533
	K_S (L mg ⁻¹)	4.9.10 ⁻⁴	4.1.10 ⁻³	3.6.10 ⁻³	8.6.10 ⁻³
	m_S	2.168	1.337	1.376	1.130
	Standard error	0.2553	0.1755	0.2114	0.2155
	R^2	0.9765	0.9870	0.9859	0.9703

The slope and intercept coefficients of the diagram of ΔG^0 (kJ mol⁻¹) versus temperature (K) gave the values of ΔH^0 and ΔS^0 , respectively. Table 7 summarizes the values of activation energy and thermodynamic parameters (ΔG^0 , ΔH^0 , and ΔS^0).

E_a was 3.63 kJ mol⁻¹, which provides an idea of the adsorption type. According to the literature, E_a lower than 40 kJ mol⁻¹ generally indicates processes controlled by diffusion; higher E_a values represent processes that involve chemical reactions (Anirudhan and Radhakrishnan 2008). The E_a value calculated herein suggested that MB adsorption was controlled by diffusion, a physical adsorption process. The negative ΔG^0 values achieved at all temperatures indicated that the process was viable and spontaneous. This parameter indicated that the process became more favorable as the temperature increased.

ΔH^0 was positive, equivalent to 88.77 kJ mol⁻¹. The standard entropy change gave the degree of disorder. The negative value of ΔS^0 (-342.63 kJ mol⁻¹ K⁻¹) indicated that the system disorder decreased at the solid/solution

interface during adsorption. According to Mohan and Singh (2002), the negative value of ΔS^0 indicates that the internal structure of the adsorbent material did not change significantly during the adsorption process.

Conclusion

Mytella falcata shells are attractive wastes with potential application in the adsorption of dyes from textile effluents, which could reduce environmental liabilities and improve environmental conditions. The use of a process to activate the shells could increase their adsorptive capacity, adding value to this product and reducing environmental problems caused by their improper disposal. FT-IR and XRD analyses confirmed the presence of calcium carbonate (CaCO₃) as aragonite and calcite in the shells. Thermal analysis (TGA) showed significant weight loss between 650 and 800 °C, a result of calcium carbonate decarbonation and calcium oxide formation. Morphological analysis evidenced the lamellar structure of

Table 7 Thermodynamics parameters

E_a (kJ mol ⁻¹)	ΔG^0 (kJ mol ⁻¹)				ΔH^0 (kJ mol ⁻¹)	ΔS^0 (J mol ⁻¹ K ⁻¹)
	298 K	313 K	323 K	333 K		
3.63	-12.36	-20.44	-21.279	-24.90	88.77	-342.63

the shells. The experimental design results demonstrated that the amount of adsorbent and the particle diameter of the adsorbent were the factors affecting adsorption the most. The best conditions to obtain maximum adsorption capacity were $M = 0.5$ g, $G < 0.149$ mm, and $A = 200$ rpm. According to the kinetic study, the adsorption equilibrium was reached in about 30 min, and the pseudo-second-order model was able to predict the kinetic data. The equilibrium studies revealed that adsorption followed the Liu model. The ΔG^0 values were negative at all temperatures, indicating a viable and spontaneous process. The ΔH^0 value was positive (32.16 kJ mol⁻¹), suggesting an endothermic process. The negative value of ΔS^0 confirmed a decreased disorder at the solid/solution interface during adsorption.

Acknowledgments The authors thank Capes, CNPq, FAPAL, and UFAL.

References

- Anirudhan TS, Radhakrishnan PG (2008) Thermodynamics and kinetics of adsorption of Cu(II) from aqueous solutions onto a new cation exchanger derived from tamarind fruit shell. *J Chem Thermodyn* 40: 702–709. doi:10.1016/j.jct.2007.10.005
- Asaoka S, Yamamoto T, Kondo S, Hayakawa S (2009) Removal of hydrogen sulfide using crushed oyster shell from pore water to remediate organically enriched coastal marine sediments. *Bioresour Technol* 100:4127–4132. doi:10.1016/j.biortech.2009.03.075
- Bharali RK, Bhattacharyya KG (2015) Biosorption of fluoride on neem (*Azadirachta indica*) leaf powder. *J Environ Chem Eng* 3:662–669. doi:10.1016/j.jece.2015.02.007
- Cardoso NF, Lima EC, Pinto IS et al (2011) Application of cupuassu shell as biosorbent for the removal of textile dyes from aqueous solution. *J Environ Manag* 92:1237–1247. doi:10.1016/j.jenvman.2010.12.010
- Carneiro PA, Umbuzeiro GA, Oliveira DP, Zanoni MVB (2010) Assessment of water contamination caused by a mutagenic textile effluent/dyehouse effluent bearing disperse dyes. *J Hazard Mater* 174:694–699. doi:10.1016/j.jhazmat.2009.09.106
- Chowdhury S, Saha P (2010) Sea shell powder as a new adsorbent to remove Basic Green 4 (Malachite Green) from aqueous solutions: equilibrium, kinetic and thermodynamic studies. *Chem Eng J* 164: 168–177. doi:10.1016/j.cej.2010.08.050
- Dauphin Y, Ball AD, Castillo-michel H, Chevillard C (2013) In situ distribution and characterization of the organic content of the oyster shell *Crassostrea gigas* (Mollusca, Bivalvia). *Micron* 44:373–383
- El Haddad M, Regti A, Laamari MR et al (2014) Calcined mussel shells as a new and eco-friendly biosorbent to remove textile dyes from aqueous solutions. *J Taiwan Inst Chem Eng* 45:533–540. doi:10.1016/j.jtice.2013.05.002
- Ezzeddine Z, Batonneau-Gener I, Pouilloux Y, Hamad H (2016) Removal of methylene blue by mesoporous CMK-3: kinetics, isotherms and thermodynamics. *J Mol Liq* 223:763–770. doi:10.1016/j.molliq.2016.09.003
- Fang J, Gao B, Zimmerman AR et al (2016) Physically (CO₂) activated hydrochars from hickory and peanut hull: preparation, characterization, and sorption of methylene blue, lead, copper, and cadmium. *RSC Adv* 6:24906–24911. doi:10.1039/C6RA01644H
- Fernandez C, Larechi MS, Callao MP (2010) An analytical overview of processes for removing organic dyes from wastewater effluents. *TrAC Trends Anal Chem* 29:1202–1211. doi:10.1016/j.trac.2010.07.011
- Foletto ELL, Weber CTT, Paz DSS et al (2012) Adsorption of leather dye onto activated carbon prepared from bottle gourd: equilibrium, kinetic and mechanism studies. *Water Sci Technol* 67:201–209. doi:10.2166/wst.2012.555
- Freundlich H (1906) Over the adsorption in solution. *J Phys Chem* 57: 358–471
- Gad HMH, El-Sayed AA (2009) Activated carbon from agricultural by-products for the removal of Rhodamine-B from aqueous solution. *J Hazard Mater* 168:1070–1081. doi:10.1016/j.jhazmat.2009.02.155
- Garrido-Rodriguez B, Cutillas-Barreiro L, Fernández-Calviño D et al (2014) Competitive adsorption and transport of Cd, Cu, Ni and Zn in a mine soil amended with mussel shell. *Chemosphere* 107:379–385. doi:10.1016/j.chemosphere.2013.12.097
- Ho YS, McKay G (1998a) Kinetic models for the sorption of dye from aqueous solution by wood. *Process Saf Environ Prot* 76:183–191. doi:10.1205/095758298529326
- Ho YS, McKay G (1998b) Sorption of dye from aqueous solution by peat. *Chem Eng J* 70:115–124. doi:10.1016/S1385-8947(98)00076-X
- Ho YS, McKay G (1999) Pseudo-second order model for sorption processes. *Process Biochem* 34:451–465. doi:10.1016/S0032-9592(98)00112-5
- Hossain A, Aditya G (2013) Cadmium biosorption potential of shell dust of the fresh water invasive snail *Physa acuta*. *J Environ Chem Eng* 1:574–580. doi:10.1016/j.jece.2013.06.030
- Hossain A, Bhattacharyya SR, Aditya G (2015) Biosorption of cadmium by waste shell dust of fresh water mussel *Lamellidens marginalis*: implications for metal bioremediation. *ACS Sustain Chem Eng* 3:1–8
- Lagergren S (1898) About the theory of so-called adsorption of soluble substances. *K Sven Vetenskapsakademiens* 24:1–39
- Langmuir I (1918) The adsorption of gases on plane surfaces of glass, mica and platinum. *J Am Chem Soc* 40:1361–1403. doi:10.1021/ja02242a004
- Li H-Y, Tan Y-Q, Zhang L et al (2012) Bio-filler from waste shellfish shell: preparation, characterization, and its effect on the mechanical properties on polypropylene composites. *J Hazard Mater* 217–218: 256–262. doi:10.1016/j.jhazmat.2012.03.028
- Liu Y, Xu H, Yang SF, Tay JH (2003) A general model for biosorption of Cd²⁺, Cu²⁺ and Zn²⁺ by aerobic granules. *J Biotechnol* 102:233–239. doi:10.1016/S0168-1656(03)00030-0
- Machado FM, Bergmann CP, Fernandes THM et al (2011) Adsorption of Reactive Red M-2BE dye from water solutions by multi-walled carbon nanotubes and activated carbon. *J Hazard Mater* 192:1122–1131. doi:10.1016/j.jhazmat.2011.06.020
- Magriotis ZM, Carvalho MZ, De Sales PF et al (2014) Castor bean (*Ricinus communis* L.) presscake from biodiesel production: an efficient low cost adsorbent for removal of textile dyes. *J Environ Chem Eng* 2:1731–1740. doi:10.1016/j.jece.2014.07.005
- Markovic S, Stankovic A, Lopacic Z et al (2015) Application of raw peach shell particles for removal of methylene blue. *J Environ Chem Eng* 3:716–724. doi:10.1016/j.jece.2015.04.002
- Matouq M, Jildeh N, Qtaishat M et al (2015) The adsorption kinetics and modeling for heavy metals removal from wastewater by Moringa pods. *J Environ Chem Eng* 3:775–784. doi:10.1016/j.jece.2015.03.027
- Mohamed M, Yousuf S, Maitra S (2012) Decomposition study of calcium carbonate in cockle shell. *J Eng Sci Technol* 7:1–10. doi:10.1007/s11440-013-0278-8
- Mohan D, Singh KP (2002) Single- and multi-component adsorption of cadmium and zinc using activated carbon derived from bagasse—an agricultural waste. *Water Res* 36:2304–2318. doi:10.1016/S0043-1354(01)00447-X
- MPA (2015) Ministério da Pesca e Aquicultura http://www.icmbio.gov.br/cepsul/images/stories/biblioteca/download/estatistica/est_2011_bol_bra.pdf. Accessed 7 Oct 2015
- OPAS (2015) Organização Pan-Americana da Saúde http://bvs.panalimentos.org/local/File/Guias_para_gerenciamento_riscos_sanitarios_em_alimentos.pdf. Accessed 8 Oct 2015

- Otero M, Cutillas-Barreiro L, Nóvoa-Muñoz JC, Arias-Estévez M, Fernández-Sanjurjo MJ, Álvarez-Rodríguez E, Núñez-Delgado A (2015) Cr(VI) sorption/desorption on untreated and mussel-shell-treated soil materials: fractionation and effects of pH and chromium concentration. *Solid Earth* 6:337–346
- Paz DS, Baiotto A, Schwaab M et al (2013) Use of papaya seeds as a biosorbent of methylene blue from aqueous solution. *Water Sci Technol* 68:441–447. doi:10.2166/wst.2013.185
- Rahimdokht M, Pajootan E, Arami M (2016) Central composite methodology for methylene blue removal by *Elaeagnus angustifolia* as a novel biosorbent. *J Environ Chem Eng* 4:1407–1416. doi:10.1016/j.jece.2016.02.006
- Redlich O, Peterson DL (1959) A useful adsorption isotherm. *J Phys Chem* 63:1024
- Russo V, Tesser R, Trifuoggi M et al (2015) A dynamic intraparticle model for fluid-solid adsorption kinetics. *Comput Chem Eng* 74: 66–74. doi:10.1016/j.compchemeng.2015.01.001
- Ruthven DM (1984) Principles of adsorption and adsorption processes, 7th edn. Springer, Berlin
- Samal K, Das C, Mohanty K (2017) Eco-friendly biosurfactant saponin for the solubilization of cationic and anionic dyes in aqueous system. *Dyes Pigments* 140:100–108. doi:10.1016/j.dyepig.2017.01.031
- Silva D, Debacher NA, Junior ABC, Rohers F (2010) Caracterização físico-química e microestrutural de conchas de moluscos bivalves provenientes de cultivos da região litorânea da ilha de Santa Catarina. *Quim Nova* 33:1053–1058
- Suzuki RM, Andrade AD, Sousa JC, Rollemberg MC (2007) Preparation and characterization of activated carbon from rice bran. *Bioresour Technol* 98:1985–1991. doi:10.1016/j.biortech.2006.08.001
- Tan IAW, Ahmad AL, Hameed BH (2008) Adsorption of basic dye using activated carbon prepared from oil palm shell: batch and fixed bed studies. *Desalination* 225:13–28. doi:10.1016/j.desal.2007.07.005
- Treviño-Cordero H, Juárez-Aguilar LG, Mendoza-Castillo DI et al (2013) Synthesis and adsorption properties of activated carbons from biomass of *Prunus domestica* and *Jacaranda mimosifolia* for the removal of heavy metals and dyes from water. *Ind Crop Prod* 42: 315–323. doi:10.1016/j.indcrop.2012.05.029
- Vieira AP, Santana SAA, Bezerra CWB et al (2009) Kinetics and thermodynamics of textile dye adsorption from aqueous solutions using babassu coconut mesocarp. *J Hazard Mater* 166:1272–1278. doi:10.1016/j.jhazmat.2008.12.043
- Viriya-empikul N, Krasae P, Puttasawat B et al (2010) Waste shells of mollusk and egg as biodiesel production catalysts. *Bioresour Technol* 101:3765–3767. doi:10.1016/j.biortech.2009.12.079
- Wang L, Li J (2013) Adsorption of C.I. Reactive Red 228 dye from aqueous solution by modified cellulose from flax shive: kinetics, equilibrium, and thermodynamics. *Ind Crop Prod* 42:153–158. doi:10.1016/j.indcrop.2012.05.031
- Webb PA, Orr C (1997) Analytical methods in fine particle technology. Micromeritics Instrument Corporation, Norcross
- Weber CT, Foletto EL, Meili L (2013) Removal of tannery dye from aqueous solution using papaya seed as an efficient natural biosorbent. *Water Air Soil Pollut*. doi:10.1007/s11270-012-1427-7
- Yao Y, Gao B, Wu F et al (2015) Engineered biochar from biofuel residue: characterization and its silver removal potential. *ACS Appl Mater Interfaces* 7:10634–10640. doi:10.1021/acsami.5b03131
- Yousefi Z, Mashayekh-Salehi A, Mohammadpour Tahmtan RA (2015) Biosorption of chromium in aqueous solutions using bivalve mollusk shells through central composite design (CCD) model. *Desalin Water Treat*:1–13. doi:10.1080/19443994.2015.1106342
- Zhang Z, O'Hara IM, Kent GA, Doherty WOS (2013) Comparative study on adsorption of two cationic dyes by milled sugarcane bagasse. *Ind Crop Prod* 42:41–49. doi:10.1016/j.indcrop.2012.05.008
- Zhou K, Yang Z, Liu Y, Kong X (2015) Kinetics and equilibrium studies on biosorption of Pb(II) from aqueous solution by a novel biosorbent: *Cyclosorus interruptus*. *J Environ Chem Eng* 3:2219–2228. doi:10.1016/j.jece.2015.08.002